Journal of Biomechanics 92 (2019) 146–154

Contents lists available at ScienceDirect

Journal of Biomechanics

journal homepage: www.elsevier.com/locate/jbiomech
www.JBiomech.com

Computational simulation of flow-induced arterial remodeling of the pancreaticoduodenal arcade associated with celiac artery stenosis

Changyoung Yuhn [a,*], Katsuyuki Hoshina [b], Kazuhiro Miyahara [b], Marie Oshima [c]

[a] Department of Mechanical Engineering, The University of Tokyo, Tokyo, Japan
[b] Department of Vascular Surgery, The University of Tokyo, Tokyo, Japan
[c] Interfaculty Initiative in Information Studies, The University of Tokyo, Tokyo, Japan

ARTICLE INFO

Article history:
Accepted 29 May 2019

Keywords:
Computational hemodynamics
Reduced-order models
Arterial remodeling
Celiac artery stenosis
Pancreaticoduodenal arcade

ABSTRACT

Arterial remodeling of the pancreaticoduodenal arcade, which enables collateral flow to the liver, spleen, and stomach, is a well-recognized clinical sign of celiac artery (CA) stenosis. However, the hemodynamic changes due to remodeling are poorly understood, despite their importance in surgical procedures such as pancreaticoduodenectomy. In this study, a framework to simulate remodeling of the arterial network following pathological flow alterations was developed and applied to investigate the hemodynamic characteristics of patients with CA stenosis. A one-dimensional–zero-dimensional cardiovascular model was used for blood flow simulation. After introducing CA stenosis into the normal network, arterial remodeling was simulated by iteratively changing the diameter of each artery until time-averaged wall shear stress reached its value under normal conditions. A representative case was simulated to validate the present framework, followed by simulation cases to investigate the impact of stenosis severity on remodeling outcome. A markedly dilated arcade was observed whose diameter agreed well with the corresponding values measured in subjects with CA stenosis, confirming the ability of the framework to predict arterial remodeling. A series of simulations clarified how the geometry and hemodynamics after remodeling change with stenosis severity. In particular, the arterial remodeling and resulting blood flow redistribution were found to maintain adequate organ blood supply regardless of stenosis severity. Furthermore, it was suggested that flow conditions in patients with CA stenosis could be estimated from geometric factors, namely, stenosis severity and arcade diameter, which can be preoperatively and non-invasively measured using diagnostic medical images.

1. Introduction

The celiac artery (CA), the first major branch of the abdominal aorta, plays a vital role in supplying oxygenated blood to the liver, spleen, and stomach. However, the CA is a common site for stenosis, typically caused by median arcuate ligament compression or atherosclerosis, with a reported incidence of 10–25% (Sakorafas et al., 2008). CA stenosis is rarely diagnosed because it is mostly asymptomatic (Song et al., 2002), owing to the existence of the pancreaticoduodenal arcade that forms a collateral pathway between the common hepatic artery (CHA) and superior mesenteric artery (SMA) (Fig. 1). With CA stenosis, the arcade undergoes remarkable dilatation, referred to as arterial remodeling, and provides compensatory collateral flow from the SMA to the organs originally supplied by the CA (Turner et al., 2014).

Despite this well-functioning collateral circulation, CA stenosis can be a serious risk factor for postoperative visceral ischemia in patients subjected to pancreaticoduodenectomy (PD), the surgical resection of tumors in the pancreas (Gaujoux et al., 2009; Nara et al., 2005), because the surgery involves resection of the arcade that could be the main supplying pathway to the CA territory. In such cases, revascularization (e.g., division of the median arcuate ligament or arterial reconstruction) during PD has been reported to prevent ischemic complications (Kurosaki et al., 2004; Nakayama et al., 2018). However, since this procedure makes surgery more complex and challenging, its necessity should be carefully assessed before implementation. The necessity may depend on the hemodynamic status of the patient, especially the amount of flow through the arcade (Gaujoux et al., 2009). Currently, a clamping test of the gastroduodenal artery (GDA) with hepatic arterial blood flow monitoring is recommended to confirm the con-

* Corresponding author at: Department of Mechanical Engineering, The University of Tokyo, De506, 4-6-1 Komaba, Meguro-ku, Tokyo 153-8505, Japan.
E-mail address: yuhn@iis.u-tokyo.ac.jp (C. Yuhn).

https://doi.org/10.1016/j.jbiomech.2019.05.043
0021-9290/

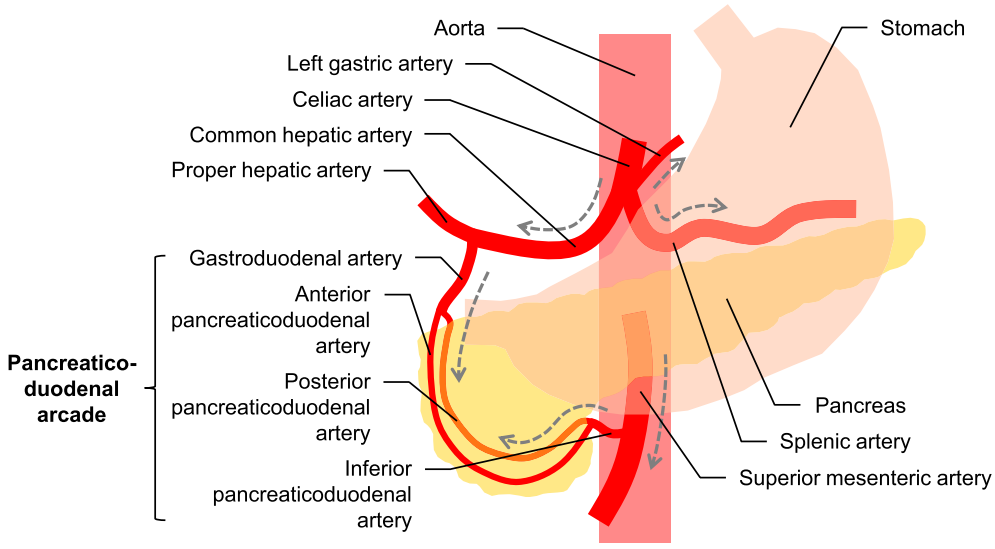

Fig. 1. Normal anatomy of the visceral arteries branching from the celiac and superior mesenteric arteries. The arrows indicate the flow directions under normal conditions.

tribution of collateral flow (Berney et al., 1998), but this test can only be conducted intraoperatively, requiring rapid judgment and decision-making. Although preoperative assessment based on stenosis severity (Sugae et al., 2012) or arcade diameter (Nakayama et al., 2018) has recently been suggested, the relationships between these geometric factors and hemodynamic conditions are not yet well understood. Therefore, detailed information about hemodynamic features, especially regarding arterial remodeling, in patients with CA stenosis can facilitate surgical planning and contribute to the selection of appropriate surgical procedures.

Computational simulations provide hemodynamic quantities under various conditions, which are usually difficult to obtain in vivo due to the invasiveness of such measurements or limited accessibility. For coupled simulation of blood flow and arterial remodeling, the constrained mixture theory extended to three-dimensional geometry is commonly employed currently (Figueroa et al., 2009; Wu and Shadden, 2015). While this framework allows the prediction of asymmetric deformation and material property changes, the computational cost of mesh generation and simulation is high. Thus, its applications tend to include only local arteries of interest with prescribed boundary conditions.

On the other hand, reduced-order modeling of the vascular network can be an efficient means of simulating a coupled problem between remodeling and the resulting boundary condition changes. In this approach, a network is modeled as interconnected segments, and growth rules are applied to individual segments through iterative calculation (Peirce and Skalak, 2003). The growth rules have been well established in previous studies (e.g., Pries et al., 1998; Reglin et al., 2009); they are designed to ensure computational stability and include experimentally obtained parameters to produce realistic networks. However, since most studies have been focused on the microvascular network, some growth factors (e.g., metabolic signals from tissues) have been considered that may not play substantial roles in large arteries (Pohl et al., 2000). Furthermore, the experimentally determined parameters are not directly applicable to larger arterial networks.

The aims of this study were therefore twofold: to construct a framework to simulate arterial network remodeling following pathological flow alterations and to investigate the hemodynamic characteristics in patients with CA stenosis by using the framework. We adopted the one-dimensional–zero-dimensional (1D–0D) cardiovascular model (Liang et al., 2009) and implemented iterative steps to simulate changes in both arterial diameter and flow distribution. Normal arterial geometries were derived from medical imaging data and literature data, and their remodeling was triggered by introducing CA stenosis. Simulations were performed with different stenosis severities to quantify the impact of stenosis severity on the results.

2. Methods

2.1. Blood flow in the cardiovascular system

The 1D–0D cardiovascular model (Liang et al., 2009; 2011) was employed for blood flow simulation, with the extension to include the visceral arteries involved in upper abdominal circulation (Fig. 2). The visceral arteries are known to exhibit many variations in their branching patterns (Song et al., 2002; 2010), but herein the model complies with normal anatomy. In this model, the 1D arterial network contains 94 segments in total. The beginning and terminal ends of the network were coupled with the 0D model representing the remaining system, forming a closed loop.

2.1.1. 1D model

A large artery was considered to be a straight and axisymmetric tube with an elastic wall, which allowed the blood flow through such an artery to be described by the equations of mass and momentum conservation (Formaggia et al., 2006; Sherwin et al., 2003):

$$\frac{\partial A}{\partial t}+\frac{\partial Q}{\partial x}=0, \tag{1}$$

$$\frac{\partial Q}{\partial t}+\frac{\partial}{\partial x}\left(\frac{Q^2}{A}\right)+\frac{A}{\rho}\frac{\partial p}{\partial x}=-K_R\frac{Q}{A}, \tag{2}$$

where x is the axial coordinate along the artery; t is the time; A, Q, and p denote the cross-sectional area, volumetric flow rate, and internal pressure, respectively; ρ is the blood density, which was taken to be 1060 kg m^{-3}; K_R is the resistance parameter modeled as $K_R = 8\pi\mu/\rho$ with blood viscosity $\mu = 0.0047$ Pa s, assuming Poiseuille flow. The relationship between pressure and cross-sectional area to close the (A, Q) system was derived assuming that arterial walls are thin, homogeneous, and purely elastic (Olufsen et al., 2000; Sherwin et al., 2003):

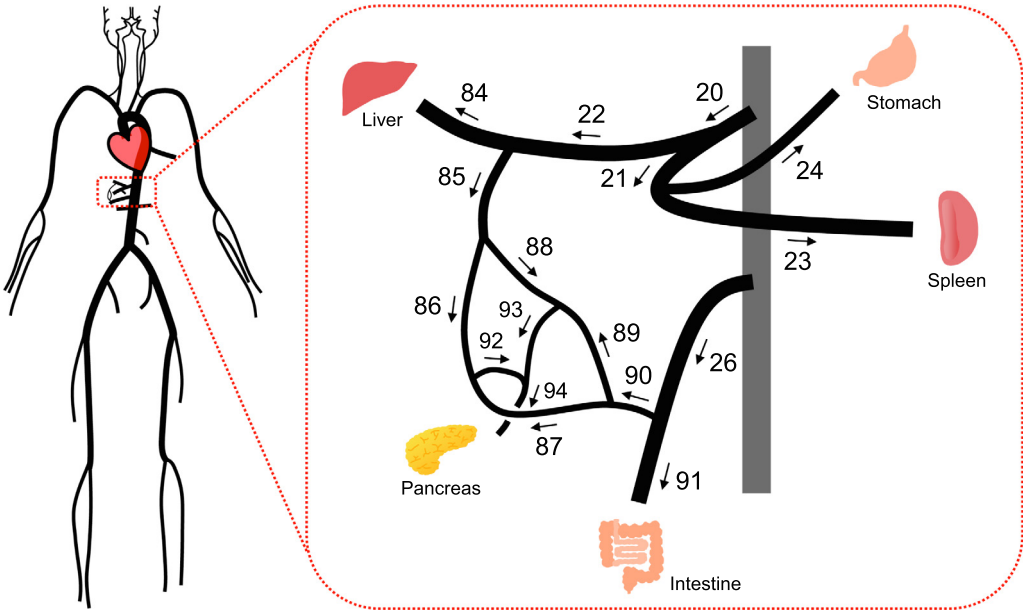

Fig. 2. Schematic representation of the 1D arterial network used in this study. The numbers refer to the arterial segments listed in Table 1, and the arrows indicate the flow directions under normal conditions. The numbering is following that established by Liang et al. (2009; 2011).

Table 1
Physiological parameters for the visceral arteries. The lengths and diameters were derived by averaging the values measured in five subjects with normal arteries. The peripheral resistances were set to distribute 3% of the cardiac output to the spleen, 1% to the stomach, 6.5% to the liver through the hepatic artery, 1% to the pancreas, and 12.5% to the intestine (Williams and Leggett, 1989).

No.	Arterial segment	Length (mm)	Diameter (mm)	Peripheral resistance (mmHg s mL^{-1})
20	Celiac I	11.26[a]	6.35	–
21	Celiac II	11.26[a]	6.35	–
22	Common hepatic	25.72	4.26	–
23	Splenic	62.18	4.25	31.67
24	Lt. gastric	30.88	2.06	86.47
26	Sup. mesenteric I	63.90	5.51	–
84	Proper hepatic	35.70	3.12	10.24
85	Gastroduodenal	29.62	2.89	–
86	Ant. sup. pancreaticoduodenal	35.61	1.34	–
87	Ant. inf. pancreaticoduodenal	35.61	1.34	–
88	Post. sup. pancreaticoduodenal	26.37	1.45	–
89	Post. inf. pancreaticoduodenal	26.37	1.45	–
90	Inf. pancreaticoduodenal	20.89	2.50	–
91	Sup. mesenteric II	17.26	4.50	6.30
92	Pancreas feeding I[b]	10.00	1.34	–
93	Pancreas feeding II[b]	10.00	1.45	–
94	Pancreas feeding III[b]	10.00	2.00	75.98

[a] Half the length of the celiac artery.
[b] Representatives of several small feeding arteries to the pancreas.

$$p - p_0 = \frac{\sqrt{\pi}Eh}{A_0(1-\sigma^2)}\left(\sqrt{A} - \sqrt{A_0}\right), \tag{3}$$

where the subscript 0 signifies the value at the reference pressure $p_0 = 85$ mmHg; h is the arterial wall thickness; and σ is Poisson's ratio (taken to be 0.5). The Young's modulus, E, was determined from curve fitting of experimental data (Olufsen et al., 2000).

2.1.2. Stenosis model

The 1D model cannot describe the pressure drop caused by flow separation and reattachment in a stenotic artery. Therefore, stenosis was modeled as presented by Young and Tsai (1973), who represented the pressure drop across stenosis as

$$\Delta p = \frac{K_v \mu}{A_n D_n} Q + \frac{K_t \rho}{2A_n^2}\left(\frac{A_n}{A_s} - 1\right)^2 Q|Q| + \frac{K_u \rho L_s}{A_n}\dot{Q}. \tag{4}$$

Here, D and L denote the artery diameter and length, respectively; $\dot{Q}$ is the time derivative of Q; n and s refer to normal and stenotic segments, respectively; and K_v, K_t, and K_u are empirical coefficients given by Seeley and Young (1976). In general, arterial stenosis is accompanied by poststenotic dilatation, as observed in Fig. 3. In Eq. (4), we defined the maximum poststenotic diameter as the normal diameter, in accordance with relevant clinical studies.

2.1.3. 0D model

The peripheral circulation was modeled as the lumped parameter (0D) network including several compartments. The compartments for the peripheral arteries (small arteries and arterioles) were represented as the three-element (RCR) Windkessel models and were coupled to the terminal arteries of the 1D model. The blood flow leaving these compartments was assumed to converge

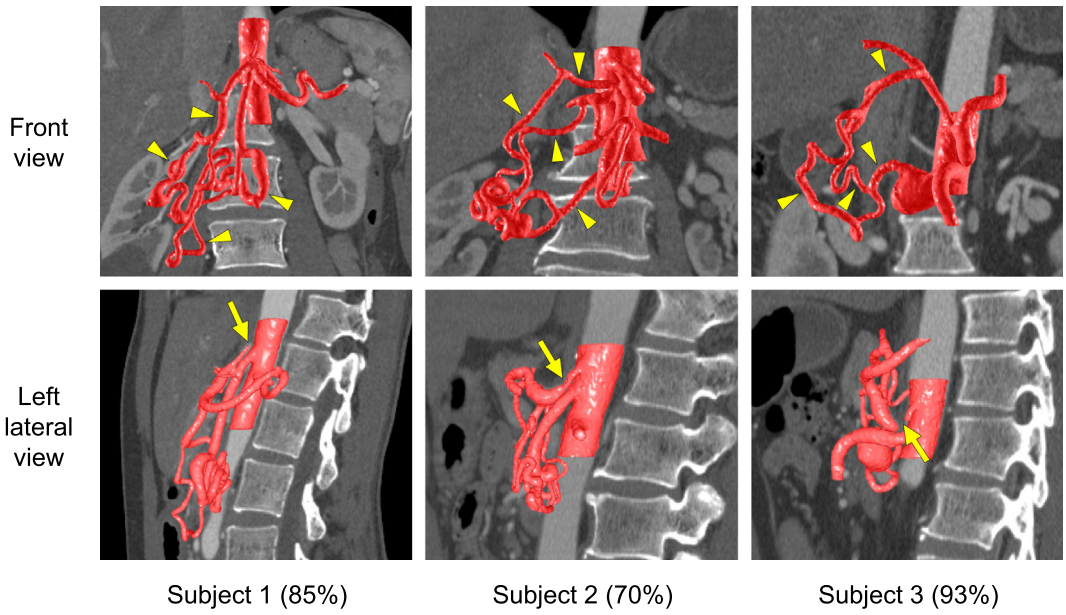

Fig. 3. Three-dimensional (3D) volume-rendered images of arterial geometry in three subjects with celiac artery stenosis (arrows). The values in parentheses indicate the stenosis severity defined as the percentage of diameter reduction. Marked dilatation of the pancreaticoduodenal arcade (arrowheads) is seen in all subjects. In-house software "V-Modeler" (Kobayashi et al., 2015) was used for 3D volume reconstruction from serial slice images.

to either upper or lower body blocks, where the compartments representing capillaries, venules, and veins were modeled as RLC series circuits. The governing equations for each compartment were given as ordinary differential equations (ODEs) derived from mass and momentum conservation (Alastruey et al., 2008; Milišić and Quarteroni, 2004). After the peripheral circulation, the blood was pumped to the ascending aorta in the 1D network according to the elastance-based heart model. For further details on the 0D model, see Liang et al. (2009).

2.1.4. Numerical methods

Eqs. (1)–(3) were solved using a two-step Lax–Wendroff scheme. The boundary values at bifurcations were calculated by enforcing mass and total pressure conservation using a Newton–Raphson method (Formaggia et al., 2006; Liang et al., 2009). The ODEs governing the 0D model were solved using a fourth-order Runge–Kutta scheme. Coupling of the models at stenosis or 1D–0D interfaces was achieved using Riemann invariants (Liang et al., 2009).

2.2. Flow-induced arterial remodeling

Arteries can change their diameters in response to altered flow conditions to maintain constant wall shear stress (WSS) (Kamiya and Togawa, 1980; Langille et al., 1989). This process was simulated by performing iterative steps in which the diameter of each 1D segment was changed every two cardiac cycles as follows:

$$D_0^{i+1} = \left(1 + \alpha^i \frac{\tau^i - \tau_h}{\tau_h}\right) D_0^i. \tag{5}$$

Here, τ is the time-averaged WSS (TAWSS); h denotes the homeostatic value; α is the relaxation coefficient; and i denotes the current iteration step. Further, the TAWSS was calculated as

$$\tau = \frac{1}{T_c} \int_0^{T_c} \frac{32\mu|Q|}{\pi D^3} dt, \tag{6}$$

where T_c is the cardiac cycle, which was fixed at 1 s. τ_h for each segment was defined as the corresponding TAWSS under normal conditions, which was obtained from blood flow simulation without stenosis.

Eq. (5) gives positive feedback if $\alpha > 0$, leading to unstable behavior of segments connected in parallel, such as Nos. 86–89 in Fig. 2 (Hacking et al., 1996; Pries et al., 1998). To avoid this problem, we permitted the diameter to change in the opposite direction by switching the sign of α according to the TAWSS gradient:

$$\alpha^i = \begin{cases} \alpha^{i-1}, & |\tau^i - \tau_h| < |\tau^{i-1} - \tau_h| \\ -\alpha^{i-1}. & |\tau^i - \tau_h| \geq |\tau^{i-1} - \tau_h| \end{cases} \tag{7}$$

Introducing Eq. (7) allows each segment to find the optimal diameter giving τ_h by changing the diameter in the direction of gradient descent. The value of α^0 can be chosen arbitrarily because it does not affect the converged diameter. In this study, the value that gave the fastest convergence without losing computational stability was used; in most cases, $\alpha^0 = 0.1$ was satisfactory, but the range was 0.05–0.15.

2.3. Numerical experiments

2.3.1. Clinical data acquisition

The geometries of the visceral arteries were collected from medical imaging data and were utilized for parameter assignment and validation of the simulated geometry. We selected eight subjects whose arteries had typical branching patterns (Fig. 1), including five subjects (two male, three female; 65.8 ± 10.7 years) with normal arteries and three subjects (one male, two female; 65.3 ± 12.4 years) with CA stenosis (Fig. 3). The length and diameter of the arteries in each subject were measured using images obtained by contrast-enhanced computed tomography. The in-plane resolution was 0.47–0.68 mm (512 × 512 pixels), and the slice thickness was 0.8 mm. All data were anonymized and provided by the University of Tokyo Hospital (Tokyo, Japan) with written informed consent from each subject. The use of the data for this study was approved by the ethics committee at our institution.

2.3.2. Parameter assignment

The physiological parameters assigned for the visceral arteries are summarized in Table 1, while those for the other arteries were taken from the literature (Liang et al., 2009; 2011). The lengths and diameters in Table 1 are the mean values of the measurements in the normal group, excepting those for Nos. 92–94, which correspond to arteries feeding the pancreas. Since peripheral resistances (the sums of two resistances in the three-element Windkessel model) dominate the flow distribution among terminal arteries (Zhang et al., 2016), they were calibrated to yield the literature values of the flow rates to adjacent organs (Williams and Leggett, 1989).

2.3.3. Simulation of representative case and validation

In the simulations, arterial network remodeling was triggered by introducing stenosis in the 1D segment (No. 20) corresponding to the CA. The stenosis was assumed to have half the length of the segment and to be located in the middle. The stenosis severity was taken to be 83% of the diameter reduction, which was the mean value for the subjects with stenosis (Fig. 3). First, the blood flow simulation was run for 10 cardiac cycles to ensure convergence. Subsequently, remodeling was begun and continued until the TAWSS reached the homeostatic value within 3% in all segments. This convergence criterion yields a diameter convergence error <1% (<0.1 mm even for the largest visceral artery) because TAWSS is inversely proportional to the cube of the diameter. For the stenotic segment, the diameter was assumed to remain constant, given that stenosis may lead to abnormality of the endothelium that senses the WSS (Zand et al., 1988).

Model validation was performed by comparing the simulated (i.e., obtained after convergence) and measured diameters. Both diameters were first normalized with respect to the aortic diameter at the CA level to exclude the effects of individual differences in arterial size, and then the normalized values were compared.

2.3.4. Impact of stenosis severity

Simulations were also performed to investigate the impact of stenosis severity on the resulting diameters and flow distribution. The stenosis severity was varied from 0% (intact artery) to 100% (complete occlusion) in 10% intervals, and 11 corresponding simu-

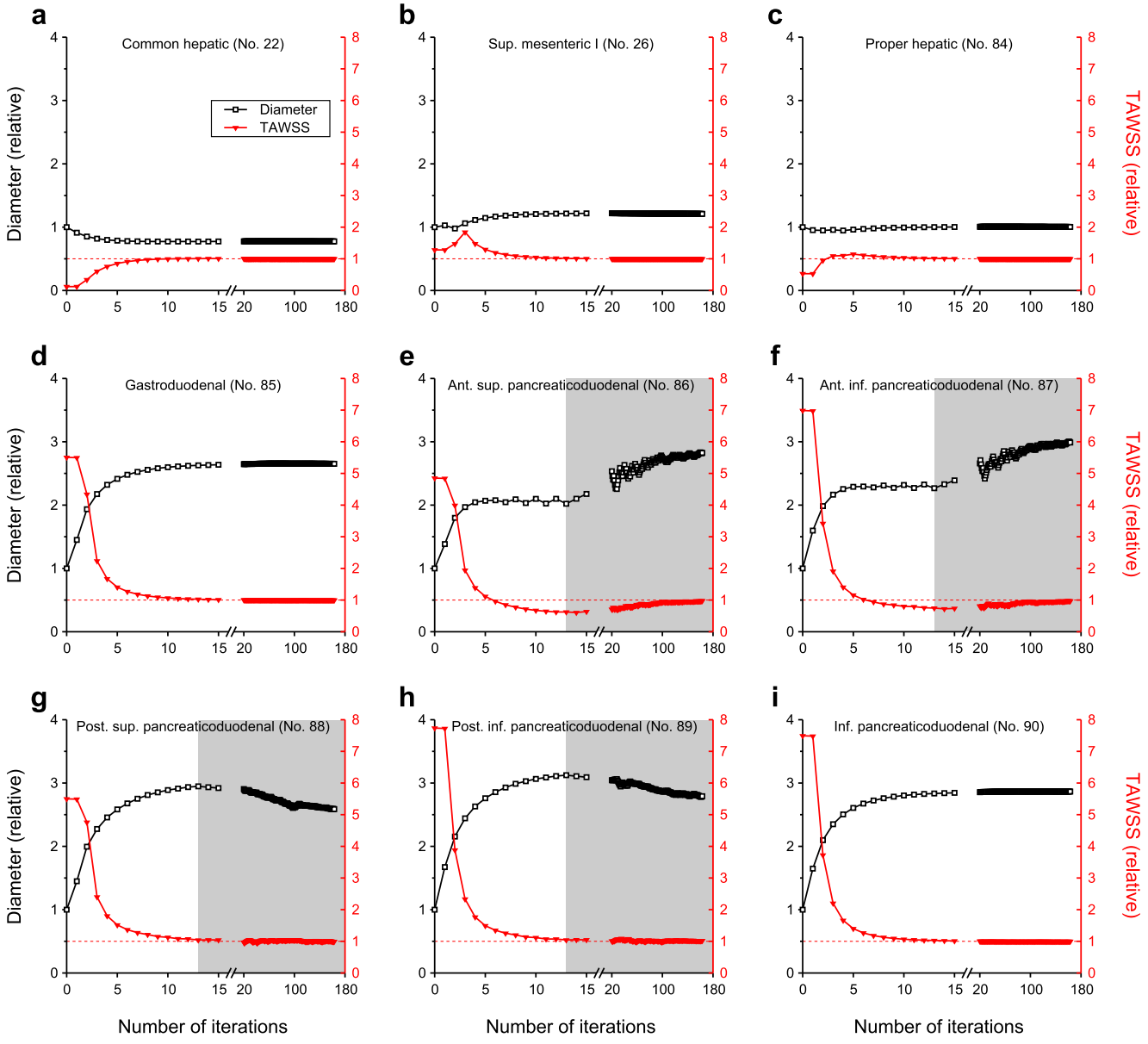

Fig. 4. Changes in diameter and time-averaged wall shear stress (TAWSS) during iterations. The diameter relative to the initial value and TAWSS relative to the homeostatic value are shown. The shaded area represents where negative feedback becomes dominant, resulting in balanced growth of arteries connected in parallel.

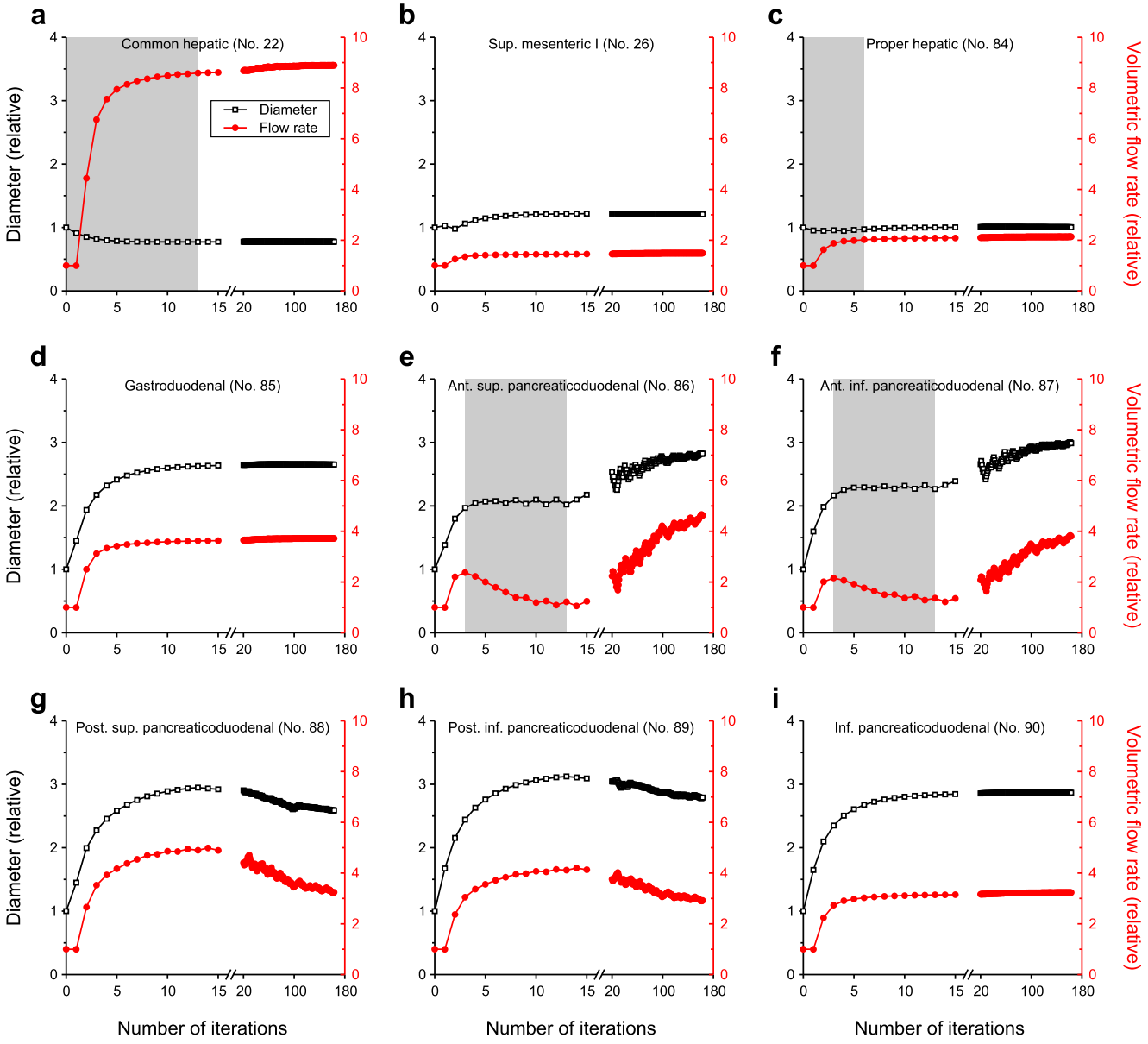

Fig. 5. Changes in diameter and cycle-averaged volumetric flow rate during iterations. The diameter and flow rate relative to their initial values are shown. The shaded area represents where a persisting change in flow rate is observed even when the diameter is stable, in contrast to synchronous changes in flow rate and diameter in the other areas.

lation cases were investigated. The case with complete occlusion was simulated by removing the CA segment from the 1D network.

3. Results

3.1. Representative case

3.1.1. Convergence behaviors

In all arteries, TAWSS values met the convergence criterion after 163 iterations of the remodeling step. The changes in diameter, TAWSS, and cycle-averaged volumetric flow rate during the iterations are summarized in Figs. 4 and 5. Here, we shall focus only on the arteries shown in the figures because the others exhibited responses similar to those of the proper hepatic artery (PHA) and yielded relatively small diameter changes (<8.7%) after convergence.

With CA stenosis introduced, the pancreaticoduodenal arcade was subjected to quite high TAWSS (Fig. 4(d)–(i)), showing more sensitive variations from the baseline than the other arteries. Subsequently, the arcade diameter increased rapidly through positive feedback of elevated TAWSS in the first few iterations. However, in the parallel pathways of the anterior and posterior pancreaticoduodenal arteries (APDA and PPDA, respectively), the diameter increased when the TAWSS was below the homeostatic value, and vice versa, during the remaining iterations (Fig. 4(e)–(h), shaded areas). Through such negative feedback, the APDA and PPDA both restored the TAWSS to the baseline and had comparable diameters.

The diameter changes were accompanied by changes in the amount of inflow (Fig. 5). Overall, the flow rate changed synchronously with the diameter. In contrast, as indicated by the shaded areas, the flow rate continued changing even when the diameter remained almost constant in arteries with inlets connected to the more drastically growing artery, namely, the APDA, whose inlet is connected to the PPDA in parallel, and the CHA and PHA, whose inlets are connected to the GDA (see Fig. 7(c) for flow directions).

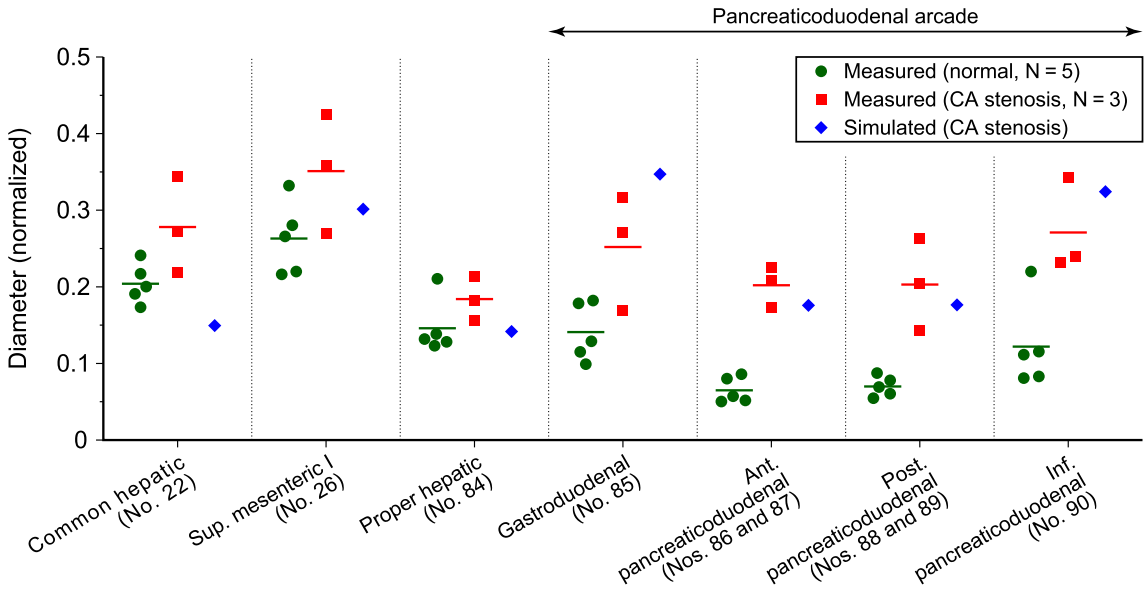

Fig. 6. Comparison of diameters between measured values in the normal and the celiac artery (CA) stenosis groups, and simulation results. The horizontal lines represent the mean values for each group. The values shown are the diameters normalized by the aortic diameter at the level of the CA.

3.1.2. Resulting diameters and blood flow distribution

Fig. 6 shows the diameters after convergence, along with those measured in the normal (N = 5) and CA stenosis (N = 3) groups. The simulation results show noticeable dilatation of the arcade, the value of which quantitatively agrees with the measurement data, where the arcades in the CA stenosis group had diameters 2–3 times as large as those in the normal group.

As expected, arterial remodeling resulted in blood flow redistribution among the arteries (Fig. 7). Upon the introduction of CA stenosis (panel b), blood flow to the organs downstream from the stenosis (i.e., liver, spleen, and stomach) decreased by half despite the formation of collateral flow from the SMA. However, owing to arterial remodeling (panel c), the flow reduction to the organs was wholly compensated by the redistributed blood flow, which was characterized by a more than threefold increase in flow through the arcade and flow reversal in the CHA.

3.2. Impact of stenosis severity on collateral circulation

Eleven additional simulation cases with different stenosis severities were examined. Fig. 8 summarizes the collateral circulation characteristics after arterial remodeling in each case. The flow rate in the PHA (i.e., blood supply to the liver) remained at a normal level regardless of stenosis severity, whereas the flow path to the liver differed. The GDA started to supply retrograde blood flow to the liver with stenosis ≥50%, and it became the single pathway supplying the liver with stenosis ≥60%, resulting in flow reversal in the CHA. The average of the diameters of APDA and PPDA drastically increased upon flow reversal in the GDA, reflecting the contribution of collateral flow to the liver.

4. Discussion

In this study, the arterial geometry restoring the TAWSS alterations caused by CA stenosis was predicted by iterative remodeling steps in 1D–0D blood flow simulations. The resulting geometry showed a markedly dilated pancreaticoduodenal arcade, reproducing a well-recognized clinical sign of CA stenosis (Sakorafas et al., 2008). Moreover, the simulated diameters agreed well with measurements in subjects with CA stenosis (Fig. 6). These results support the widely accepted concept that arteries maintain constant levels of mechanical stimuli, WSS in this case, by structurally adapting to the altered hemodynamic conditions (see a review by Humphrey (2008)).

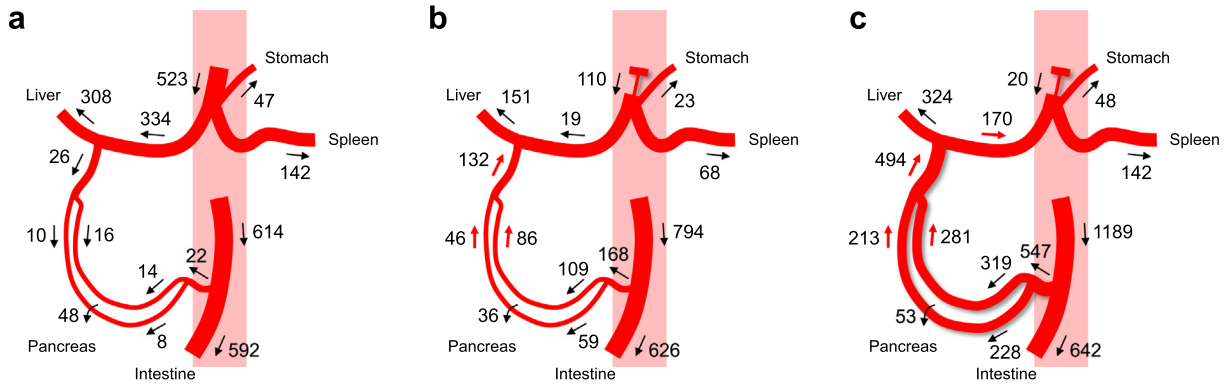

Fig. 7. Comparison of cycle-averaged volumetric flow rates (mL/min) and flow directions between three conditions: (a) normal, (b) immediately after introducing celiac artery stenosis, (c) at the end of remodeling. The red arrows indicate flow reversal from the normal state. (For interpretation of the references to color in this figure legend, the reader is referred to the web version of this article.)

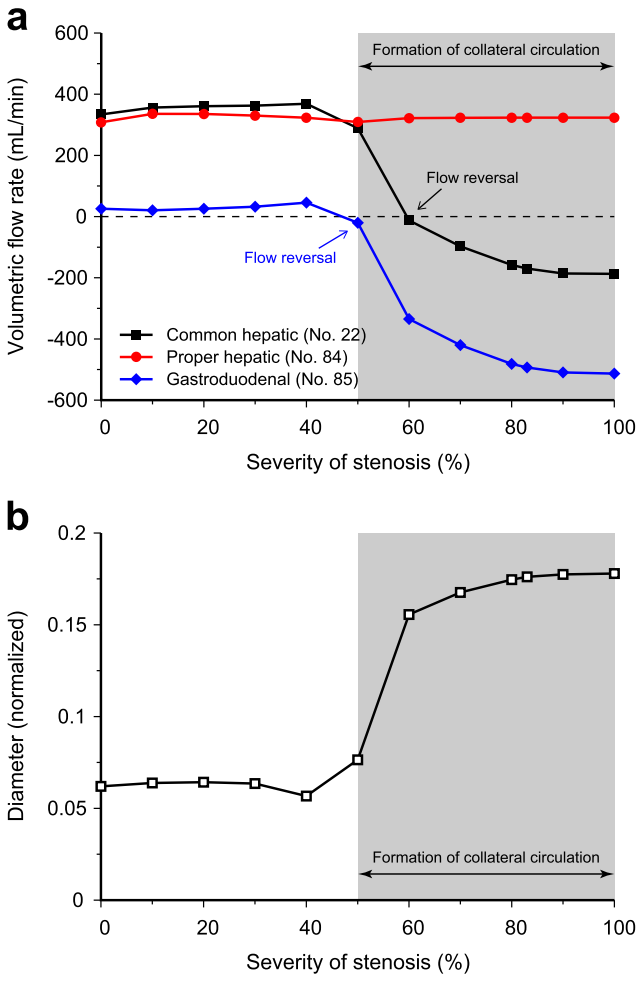

Fig. 8. Impact of stenosis severity (percentage of diameter reduction) on collateral circulation after arterial remodeling: (a) cycle-averaged volumetric flow rates in the common hepatic, proper hepatic, and gastroduodenal arteries, (b) average of the diameters of the anterior and posterior pancreaticoduodenal arteries. The negative flow rates represent flow reversal from the normal state. The diameter shown is the value normalized by the aortic diameter at the level of the celiac artery.

Although the underlying goal of remodeling (i.e., normalizing the altered TAWSS) appears simple, it is difficult to achieve computationally for arteries in a network. For a single isolated artery, it appears reasonable to assume a positive feedback system (Manini et al., 2014; Taber, 1998), which restores the elevated TAWSS by increasing the diameter, and vice versa (see Eq. (6)). However, when the arteries form a network, a diameter change in one artery will influence the flow (and thereby the TAWSS) in the neighboring arteries. For instance, the flow into the APDA continued decreasing while the diameter remained constant (Fig. 5(e) and (f)), being affected by the PPDA, which grew faster and therefore received more flow at the bifurcation (Fig. 5(g) and (h)). Likewise, the CHA and PHA restored TAWSS due to the remarkably increased flow from the upstream arcade rather than changing diameters themselves (Fig. 5(a) and (c)). Under such mutual influence, diameter control solely by positive feedback does not allow TAWSS restoration in every artery in the network (Hacking et al., 1996; Pries et al., 1998).

To address this issue, we regarded the remodeling of each artery as an optimization process involving minimizing the deviation of the TAWSS from the homeostatic value. The diameter was controlled by either positive or negative feedback to follow the direction of gradient descent of the deviation. Our simulation thereby yielded stable convergence because each artery, under the mutual influence, changed diameter in a manner favorable to TAWSS restoration (Fig. 4). Unlike previous studies (Pries et al., 1998; Reglin et al., 2009) in which metabolic signals were considered crucial to stabilizing the diameter response, we assumed the TAWSS to be the single factor inducing the response, considering that large arteries are far from tissues sending such signals (Pohl et al., 2000). Therefore, our approach does not require determining parameters experimentally to set the balance between growth factors.

Interestingly, even though remodeling was a process for individual arteries that involved the use of only local information, it yielded the network optimal for supplying normal blood volume to the organs (Fig. 7). Moreover, this trend was observed regardless of stenosis severity (Fig. 8(a)), indicating that the functioning of the arterial network is robustly maintained via local adaptation. These results suggest that the arteries form a branching pattern in which local WSS maintenance has the same effect as maintaining the function of the whole network (Kamiya et al., 1984). Furthermore, given that the constant WSS concept originated from the principle of minimum work for blood circulation (Murray, 1926), the results can be interpreted as indicating that the network expends less energy when it distributes the limited cardiac output to the destinations exactly as demanded.

The results in Fig. 8 reveal the relationships between the geometric and hemodynamic features, enabling estimation of flow condition based on stenosis severity or arcade diameter. In clinical PD practice, a common criterion for performing additional revascularization appears to be hepatic arterial flow reduction when the GDA is clamped (Gaujoux et al., 2009; Nara et al., 2005). Our results showed that this criterion corresponds to CA stenosis $\geq$50% and the APDA/PPDA having a normalized diameter $\geq$0.076, providing the geometry-based criteria. These criteria are in line with surgical strategies proposed in retrospective chart review studies (Nakayama et al., 2018; Sugae et al., 2012), further supporting them with the underlying hemodynamic features. Since geometric factors can be obtained preoperatively and non-invasively from diagnostic medical images, our findings could assist surgeons in predicting the necessity of revascularization and preparing for required procedures.

While this study provided quantitative insights into the hemodynamic features of patients with CA stenosis, it has some limitations. First, anatomical variations of the visceral arteries, especially the existence of other collateral pathways (Song et al., 2002), may affect the results for moderate stenosis (40–60%), where drastic changes in the flow through the GDA were observed (Fig. 8). Indeed, it might be for this reason that the GDA flow measurements varied notably between patients with moderate stenosis (Haquin et al., 2017). Second, in reality, not only the arcade diameter but also arcade length and wall thickness change, which result in elongated and tortuous shapes (Fig. 3) and material property changes. Nevertheless, we do not anticipate that the remodeling neglected herein will significantly affect the results, because wall properties do not affect flow resistance, and the impact of length on flow resistance is much less than that of diameter (first power vs. fourth power, respectively). Third, we assumed that the endothelium perfectly restores TAWSS to the homeostatic value. However, factors such as age, inflammatory diseases, and oxidative stress can cause endothelial dysfunction (Wu et al., 2014), which can lead to suboptimal remodeling. Finally, depending on the relaxation coefficient, the gradient descent may converge to a local stationary point before reaching the homeostatic value.

5. Conclusion

We demonstrated that flow-induced remodeling of the arterial network could be predicted numerically by introducing iterative

remodeling steps into a 1D–0D blood flow simulation. The iterations using the gradient descent of the TAWSS yielded stable convergence even for arteries whose responses were affected mutually. Our results showed that, regardless of CA stenosis severity, the local adaptation of arteries redistributes blood flow among them and consequently maintains adequate blood supply to the organs. Furthermore, we revealed how the remodeling outcome changes with stenosis severity, relating the flow features to geometric factors. These findings are expected to facilitate preoperative risk assessment and surgical planning, leading to safer surgical treatment of patients with CA stenosis.

Acknowledgements

This work was supported by the Japan Society for the Promotion of Science through Grants-in-Aid for Scientific Research (Grant Nos. 16H04264 and 18J21374).

Conflict of interest statement

The authors have no conflicts of interest to declare.

References

Alastruey, J., Moore, S.M., Parker, K.H., David, T., Peiró, J., Sherwin, S.J., 2008. Reduced modelling of blood flow in the cerebral circulation: coupling 1-D, 0-D and cerebral auto-regulation models. Int. J. Numer. Meth. Fluids 56, 1061–1067.

Berney, T., Pretre, R., Chassot, G., Morel, P., 1998. The role of revascularization in celiac occlusion and pancreatoduodenectomy. American J. Surgery 176, 352–356.

Figueroa, C.A., Baek, S., Taylor, C.A., Humphrey, J.D., 2009. A computational framework for fluid-solid-growth modeling in cardiovascular simulations. Comput. Methods Appl. Mech. Eng. 198, 3583–3602.

Formaggia, L., Lamponi, D., Tuveri, M., Veneziani, A., 2006. Numerical modeling of 1D arterial networks coupled with a lumped parameters description of the heart. Comput. Methods Biomech. Biomed. Eng. 9, 273–288.

Gaujoux, S., Sauvanet, A., Vullierme, M.P., Cortes, A., Dokmak, S., Sibert, A., Vilgrain, V., Belghiti, J., 2009. Ischemic complications after pancreaticoduodenectomy: incidence, prevention, and management. Ann. Surg. 249, 111–117.

Hacking, W.J., VanBavel, E., Spaan, J.A., 1996. Shear stress is not sufficient to control growth of vascular networks: a model study. American J. Physiol. Heart Circulatory Physiol. 270, H364–H375.

Haquin, A., Sigovan, M., Si-Mohamed, S., Mabrut, J.Y., Manichon, A.F., Bakir, M., Rode, A., Boussel, L., 2017. Phase-contrast MRI evaluation of haemodynamic changes induces by a coeliac axis stenosis in the gastroduodenal artery. British J. Radiol. 90, 20160802.

Humphrey, J.D., 2008. Vascular adaptation and mechanical homeostasis at tissue, cellular, and sub-cellular levels. Cell Biochem. Biophys. 50, 53–78.

Kamiya, A., Bukhari, R., Togawa, T., 1984. Adaptive regulation of wall shear stress optimizing vascular tree function. Bull. Math. Biol. 46, 127–137.

Kamiya, A., Togawa, T., 1980. Adaptive regulation of wall shear stress to flow change in the canine carotid artery. American J. Physiol. Heart Circulat. Physiol. 239, H14–H21.

Kobayashi, M., Hoshina, K., Yamamoto, S., Nemoto, Y., Akai, T., Shigematsu, K., Watanabe, T., Ohshima, M., 2015. Development of an image-based modeling system to investigate evolutional geometric changes of a stent graft in an abdominal aortic aneurysm. Circ. J. 79, 1534–1541.

Kurosaki, I., Hatakeyama, K., Nihei, K.E., Oyamatsu, M., 2004. Celiac axis stenosis in pancreaticoduodenectomy. J. Hepato-Biliary-Pancreat. Surgery 11, 119–124.

Langille, B.L., Bendeck, M.P., Keeley, F.W., 1989. Adaptations of carotid arteries of young and mature rabbits to reduced carotid blood flow. American J. Physiol. Heart Circulat. Physiol. 256, H931–H939.

Liang, F., Takagi, S., Himeno, R., Liu, H., 2009. Multi-scale modeling of the human cardiovascular system with applications to aortic valvular and arterial stenosis. Med. Biol. Eng. Compu. 47, 743–755.

Liang, F., Fukasaku, K., Liu, H., Takagi, S., 2011. A computational model study of the influence of the anatomy of the circle of Willis on cerebral hyperperfusion following carotid artery surgery. BioMed. Eng. OnLine 10, 84.

Manini, S., Passera, K., Huberts, W., Botti, L., Antiga, L., Remuzzi, A., 2014. Computational model for simulation of vascular adaptation following vascular access surgery in haemodialysis patients. Comput. Meth. Biomech. Biomed. Eng. 17, 1358–1367.

Milišić, V., Quarteroni, A., 2004. Analysis of lumped parameter models for blood flow simulations and their relation with 1D models. Math. Model. Numerical Anal. 38, 613–632.

Murray, C.D., 1926. The physiological principle of minimum work. I. The vascular system and the cost of blood volume. PNAS 12, 207–214.

Nakayama, Y., Sugimoto, M., Kobayashi, T., Gotohda, N., Takahashi, S., Kusumoto, M., Konishi, M., 2018. Impact of pancreaticoduodenal arcade dilation on postoperative outcomes after pancreaticoduodenectomy. HPB 20, 49–56.

Nara, S., Sakamoto, Y., Shimada, K., Sano, T., Kosuge, T., Takahashi, Y., Onaya, H., Yamamoto, J., 2005. Arterial reconstruction during pancreatoduodenectomy in patients with celiac axis stenosis—utility of Doppler ultrasonography. World J. Surg. 29, 885–889.

Olufsen, M.S., Peskin, C.S., Kim, W.Y., Pedersen, E.M., Nadim, A., Larsen, J., 2000. Numerical simulation and experimental validation of blood flow in arteries with structured-tree outflow conditions. Ann. Biomed. Eng. 28, 1281–1299.

Peirce, S.M., Skalak, T.C., 2003. Microvascular remodeling: a complex continuum spanning angiogenesis to arteriogenesis. Microcirculation 10, 99–111.

Pohl, U., De Wit, C., Gloe, T., 2000. Large arterioles in the control of blood flow: role of endothelium-dependent dilation. Acta Physiologica Scandinavica 168, 505–510.

Pries, A.R., Secomb, T.W., Gaehtgens, P., 1998. Structural adaptation and stability of microvascular networks: theory and simulations. American J. Physiol. Heart Circulat. Physiol. 275, H349–H360.

Reglin, B., Secomb, T.W., Pries, A.R., 2009. Structural adaptation of microvessel diameters in response to metabolic stimuli: where are the oxygen sensors? American J. Physiol. Heart Circulat. Physiol. 297, H2206–H2219.

Sakorafas, G.H., Sarr, M.G., Peros, G., 2008. Celiac artery stenosis: an underappreciated and unpleasant surprise in patients undergoing pancreaticoduodenectomy. J. Am. Coll. Surg. 206, 349–356.

Seeley, B.D., Young, D.F., 1976. Effect of geometry on pressure losses across models of arterial stenoses. J. Biomech. 9, 439–448.

Sherwin, S.J., Franke, V., Peiró, J., Parker, K., 2003. One-dimensional modelling of a vascular network in space-time variables. J. Eng. Math. 47, 217–250.

Song, S.Y., Chung, J.W., Kwon, J.W., Joh, J.H., Shin, S.J., Kim, H.B., Park, J.H., 2002. Collateral pathways in patients with celiac axis stenosis: angiographic–spiral CT correlation. RadioGraphics 22, 881–893.

Song, S.Y., Chung, J.W., Yin, Y.H., Jae, H.J., Kim, H.C., Jeon, U.B., Cho, B.H., So, Y.H., Park, J.H., 2010. Celiac axis and common hepatic artery variations in 5002 patients: systematic analysis with spiral CT and DSA. Radiology 255, 278–288.

Sugae, T., Fujii, T., Kodera, Y., Kanzaki, A., Yamamura, K., Yamada, S., Sugimoto, H., Nomoto, S., Takeda, S., Nakao, A., 2012. Classification of the celiac axis stenosis owing to median arcuate ligament compression, based on severity of the stenosis with subsequent proposals for management during pancreatoduodenectomy. Surgery 151, 543–549.

Taber, L.A., 1998. A model for aortic growth based on fluid shear and fiber stresses. J. Biomech. Eng. 120, 348–354.

Turner, K.M., Majekodunmi, K., Manejwala, A., Neschis, D., Novak, Z., Boutros, C., 2014. Image findings in celiac artery stenosis due to median arcuate ligament compression: a crucial diagnosis when planning for pancreaticoduodenectomy. J. Gastrointest. Surgery 18, 638–640.

Williams, L.R., Leggett, R.W., 1989. Reference values for resting blood flow to organs of man. Clin. Phys. Physiol. Meas. 10, 187–217.

Wu, J., Shadden, S.C., 2015. Coupled simulation of hemodynamics and vascular growth and remodeling in a subject-specific geometry. Ann. Biomed. Eng. 43, 1543–1554.

Wu, J., Xia, S., Kalionis, B., Wan, W., Sun, T., 2014. The role of oxidative stress and inflammation in cardiovascular aging. BioMed. Res. Int. 2014, 615312.

Young, D.F., Tsai, F.Y., 1973. Flow characteristics in models of arterial stenoses—II. unsteady flow. J. Biomech. 6, 547–559.

Zand, T., Nunnari, J.J., Hoffman, A.H., Savilonis, B.J., MacWilliams, B., Majno, G., Joris, I., 1988. Endothelial adaptations in aortic stenosis. correlation with flow parameters. American J. Pathol. 133, 407–418.

Zhang, H., Fujiwara, N., Kobayashi, M., Yamada, S., Liang, F., Takagi, S., Oshima, M., 2016. Development of a numerical method for patient-specific cerebral circulation using 1D–0D simulation of the entire cardiovascular system with SPECT data. Ann. Biomed. Eng. 44, 2351–2363.